Semnan University

Progress in Physics of Applied Materials

journal homepage: https://ppam.semnan.ac.ir/

Structural, Surface Morphological, and Optical Properties of Pulsed Laser Deposited MoS_2/ZnO Microrods for Optoelectronic Applications

Ahmad Kamalianfar [a*], Mahmoud Naseri [b]

[a] *Department of Physics Education, Farhangian University, P.O. Box 14665-889, Tehran, Iran*

[b] *Department of Physics, Faculty of Science, Malayer University, Malayer, Iran*

ARTICLE INFO

Article history:
Received: 25 November 2024
Revised: 13 January 2025
Accepted: 13 January 2025

Keywords:
Optoelectronic;
MoS_2;
PLD Method;
MoS_2/ZnO Composite.

ABSTRACT

In the present work, hexagonal MoS_2/ZnO thin film was synthesized via pulsed laser deposition method. We studied the structural and optical properties of MoS_2/ZnO thin film deposited on Si (100) substrate at room temperature using a Nd:YAG laser (248 nm, 10 ns pulse duration and 10 Hz repetition rate). FESEM images demonstrated a flower-like topography of MoS_2/ZnO with the well-defined hexagonal microrods and flat top surface. The band gap was determined from the analysis of UV-Visible spectrum and found to be 2.90 eV for MoS_2/ZnO microrods and 3.12 eV for pure ZnO. The hexagonal wurtzite crystal structure of MoS_2/ZnO composite thin film was confirmed by XRD pattern. Raman spectrum of MoS_2/ZnO microrods showed two characteristics peaks at 379 and 403 cm^{-1}corresponding to E^1_{2g} and A_{1g} modes, respectively. Enhancement of the near-band-edge ultraviolet emission was achieved by deposition of MoS_2 on the surface of ZnO microrods. The Ossila four-point probe device measured the DC electrical conductivity. The results indicate that MoS_2/ZnO microrods are regarded as promising prospects for the future of optoelectronic applications.

1. Introduction

Metal oxides possess a wide range of applications in optical devices, catalysts, sensors, fuel cells, batteries, and supercapacitors. Among metal oxides, the large exciton binding energy and bandgap of Zinc oxide ensures its suitability for optoelectronic applications at room temperature [1]. Zinc oxide has been found a promising material for laser diodes [2], ultraviolet (UV) light emitting diodes [3], sensors [4], and many more.

As a promising candidate for future optoelectronic applications, the noble metal-ZnO composites have been extensively investigated because it is one promising way of tuning the optical, electronic, and magnetic characteristics of zinc oxide semiconductor [5-8]. Although decorating and doping ZnO with metals and transition metals can improve its optical properties, the high cost and scarcity of this metal limit its application in the field of optoelectronic engineering.

On the other hand, transition metal dichalcogenides (MoS_2, $MoSe_2$ and WS_2) have attracted more and more attention in the field in optoelectronic device applications [9-11]. Among them, molybdenum disulfide has been extensively studied in various electronic and optoelectronic devices due to its unique electrical, physical, and chemical properties [12]. Its two-dimensional (2D) layered structure gives high specific surface energy and good electronic conductivity [13]. The layers of Mo-atom and S-atoms are connected by weak van der Waals interactions forming a trigonal prismatic or octahedral structure. Despite all these advantages, pure MoS_2 suffers from the fast electron-hole recombination due to its high specific surface energy. To overcome this drawback, several studies have suggested formation of nanocomposite of ZnO with MoS_2 sheets. For

* Corresponding author. Tel.: +98-917-0522588
E-mail address: A.kamalianfar@cfu.c.ir, Kamalianfar.ahmad@gmail.com

Cite this article as:
Kamalianfar A. and Naseri M., 2025. Structural, Surface Morphological, and Optical Properties of Pulsed Laser Deposited MoS_2/ZnO Microrods for Optoelectronic Applications. *Progress in Physics of Applied Materials*, *5*(1), pp.67-73. DOI: **10.22075/PPAM.2025.35870.1121**

example, a simple dual step hydrothermal reduction method has been used for the synthesis of molybdenum disulphide-zinc oxide (MoS_2/ZnO) nanocomposites for industrial pollutants [14]. Tang et al. prepared MoS_2/ZnO composite via simple co-precipitation method. The synthesized samples showed the enhancement in photocatalytic performance [15]. Hai-Quan Liu et al. reported that the MoS_2/ZnO composite films were successfully prepared by using magnetron sputtering method, which is considered the excellent linear-nonlinear absorption characteristic [16]. To the best of the author's knowledge, only few studies been conducted to investigate decoration of transition metal dichalcogenides on ZnO nanorods.

In this work, we present fabrication and studies of pure ZnO and MoS_2/ZnO microrods in view of optoelectronic application.

2. Experimental Setup, Method and Equipment

In this study, ZnO films were deposited on Si (111) substrate from a ZnO target (ZnO purity 99.99%) by pulsed laser deposition using a Nd: YAG laser (λ = 248 nm, FWHM pulse duration of 10 ns). The base pressure was 5×10^{-7} Torr in the chamber, pure hydrogen gas was fed into the chamber at pressures in the range of 50–200 mTorr. Deposition was carried out for 15 min at a target-substrate distance of about 20 cm. Two-inch diameter MoS_2 target (99.99%) was used to deposit MoS_2 multilayer film on the ZnO microrods. The deposition of MoS_2 film was carried out for 10 min at a target-substrate distance of ~10 cm. The substrate temperature was set at 700 °C. The sample then was annealed at 200-400 °C in air for a period of 2 hours. More experimental setup is described in detail in Ref. [17]. The sample thus prepared is referred to as MoS_2/ZnO.

3. Characterization

The structural properties of synthesized nanoparticles were investigated by Shimadzu XRD 6000 employing CuKe (0.154 nm) radiation. Morphologies of samples were observed under field emission scanning electron microscope (FESEM, JSM-6700F). Optical absorption spectrum was recorded on a Perkin Elmer Lambda 360 shimadzu UV-Vis. Photoluminescence measurement was recorded on a fluorescence spectrometer (LS 55, a Xenon lamp with an excitation wavelength of 325 nm), while Raman spectrum of the sample was measured with a Raman spectrometer (Renishaw in Via with λ = 514 nm laser excitation) at room temperature.

The electrical conductivity (EC) was measured using an Ossila four-point probe. The experimental arrangement is shown in Fig. 1, where S denotes the spacing between the equidistant probes. Besides, two of the probes were connected to source current (I) and the other two probes were used to measure voltage (V) by two-channel Model 2182A nano voltmeter. The electrical conductivity, σ, is given by $\sigma = {}^{I}/_{2\pi VS}$.

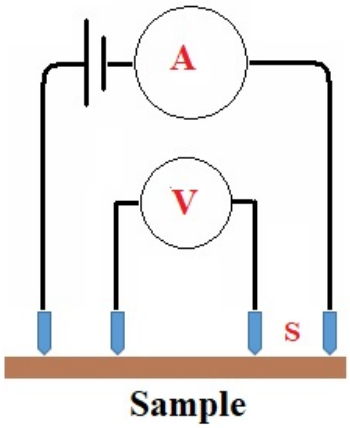

Fig. 1. Four- point- probe method

4. Results and Discussion

4.1.X-Ray Diffraction (XRD) Analysis

The diffraction peaks in XRD patterns of pure ZnO and MoS2/ZnO microrods are presented in Fig. 2. The X-ray diffraction results as well confirmed the formation of hexagonal wurtzite structure of ZnO (compared with JCPDS 36–1451) with peaks corresponding to (100), (002), (101), (102), and (110) planes.

A new diffraction peak located at about 2θ=14.38° appears in the XRD pattern of MoS2/ZnO composite in comparison to pure ZnO microrods. This diffraction peak can be assigned to hexagonal MoS2 phase by comparing with the standard data from JCPDS card No. 06-0097.

The Debye Scherrer equation is used to calculate the crystallite size [18]:

$$D = {}^{0.9\,\lambda}/_{\beta \cos\theta} \qquad (1)$$

where β is the full width at half-maximum (FWHM), k is the Scherrer constant, D is the crystallite size, and λ denotes the wavelength of monochromatic Cu-Kα radiation (1.54 Å). The values of crystallite size of pure ZnO and MoS_2/ZnO composite were determined to be about 32 nm and 43, respectively.

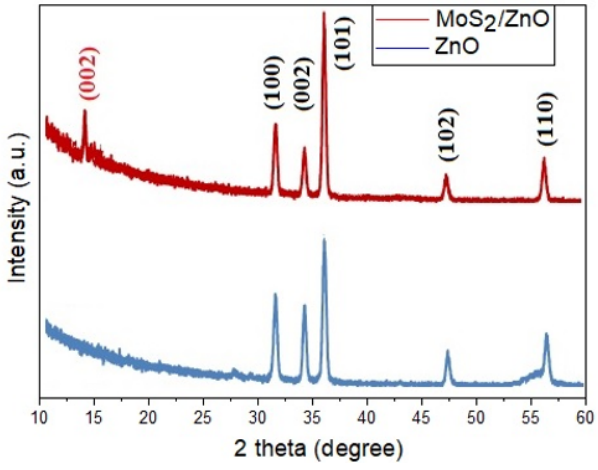

Fig. 2. XRD patterns of pure ZnO and MoS2/ZnO thin films

4.2. Surface Properties of MoS_2/ZnO

An advanced technology called field emission scanning electron microscopy (FE-SEM) is used for analyzing the microstructure and morphology of materials. Fig. 3 shows the FESEM images of the surface morphology of pure ZnO and MoS_2/ZnO samples. Fig. 3a clearly reveals a flower-like topography of ZnO with the well-defined hexagonal microrods and flat top surface. The microrods originated from same nucleating centers, which grew almost perpendicular to the substrate. Although the diameter and length of the microrods are not the same in each flower-like microstructures, but for the image shown, the diameter of the flat top surface of the hexagonal microrods is in the range of about 1 μm while their length is 1–2 μm.

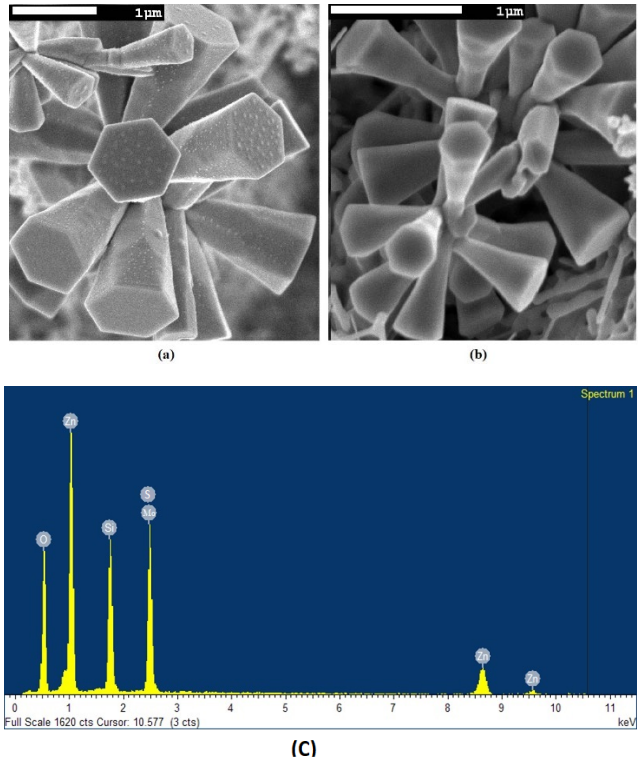

Fig. 3. FESEM images of (a) pure ZnO, (b) MoS_2/ZnO, and (c) EDX image of MoS_2/ZnO thin films

In comparison to pure ZnO thin film, the surface of MoS_2/ZnO microrods shows more roughness and distortion as observed in Fig. 3b. The diameter of the hexagonal MoS_2/ZnO microrods ranges between 300 and 400 nm, while their typical length achievable is 0.5–1 μm.

Information about the elemental composition of the sample was further conducted using the energy-dispersive x-ray analysis (EDX) as shown in Fig 3c. Presence of Mo, S, Zn, O, and Si was observed supporting the formation of MoS_2/ZnO on Si substrate. The vibrational modes of atoms in pure ZnO and MoS_2/ZnO were studied using Raman spectroscopy in the range 200–700 cm^{-1}. As shown in Fig. 4, the Raman spectrum of ZnO microrods reveals a strong E2 high-frequency mode peak at nearly ~438 cm^{-1}, which confirms the wurtzite structure of zinc oxide [18]. This peak can be related to nonpolar vibration mode caused by Zn lattice motion. The Raman spectrum of MoS_2/ZnO showed peaks at 378 and 402 cm^{-1} assigned to E^1_{2g} and A_{1g} modes, respectively. The out-of-plane A_{1g} mode and the in-plane vibration E^1_{2g} mode represent the transverse vibrations of the two S atoms and longitudinal vibrations of Mo and S atoms in opposite directions towards each other, respectively [19]. These findings indicate MoS_2 is successfully deposited on ZnO microrods [20].

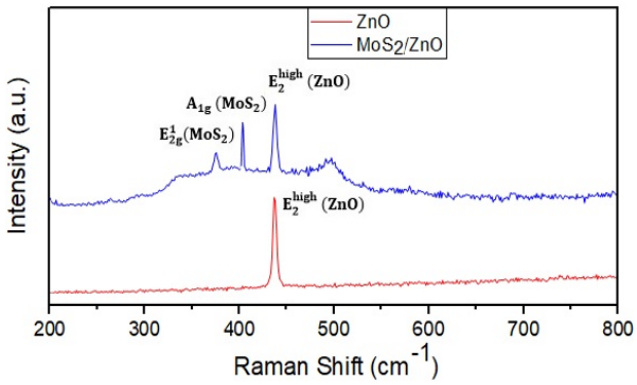

Fig. 4. Raman spectra of pure ZnO and MoS_2/ZnO thin films

4.3. UV–vis absorption spectroscopy

UV-visible spectroscopy is used to study the optical characteristics of the pure ZnO and MoS_2/ZnO samples. Fig. 5 exhibits UV-Vis absorption spectrum in the 300–700 nm range. Two samples exhibited high absorption in the UV region, with a strong absorption around 370–395 witch is assigned to Zn-O bonding in wurtzite ZnO [21].

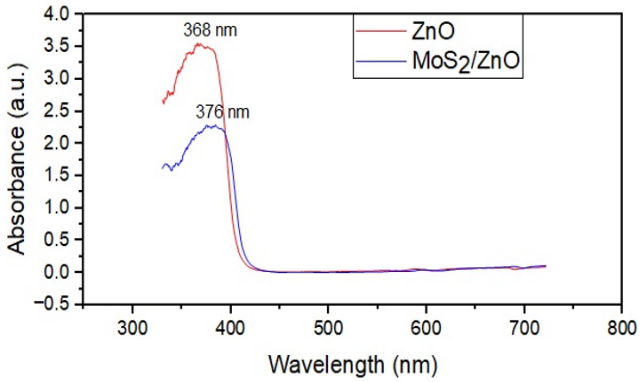

Fig. 5. The UV–Vis absorption spectrums of pure ZnO and MoS_2/ZnO thin films

The presence of MoS_2 element changes the electronic band structure energy of MoS_2/ZnO sample. Decoration of MoS_2 on ZnO microrods makes it easier for electrons to transfer and boost charge transfer lifetime in MoS_2/ZnO sample. In addition, the presence of an exposed S atom edge in the sample can boost more light responsive area and provide the enhanced optical absorption [22].

Compared with pure ZnO sample, the optical absorption of MoS_2/ZnO exhibited red shift in the absorption edge. The red shift is attributed to the contribution of MoS_2 (as foreign atoms) in the lattice and the difference in the primitive cell of ZnO and MoS_2 [23].

The band gap energy is usually determined from the following equation [24]:

$$\alpha h\nu = A(h\nu - E_g)^{1/2} \quad (2)$$

where E_g is the average band gap of the material, A is a constant, hν is the energy of photon, and α is the absorption coefficient.

Fig. 6 shows the bandgap as a function of incident laser energy. The estimated bandgaps of ZnO and MoS_2/ZnO samples are listed in Table 1. Smaller the optical band gap energy, larger should be the particle size. Thus, because of the crystalline nature of the thin films, an apparent increase in the band gap results in the smaller grain sizes.

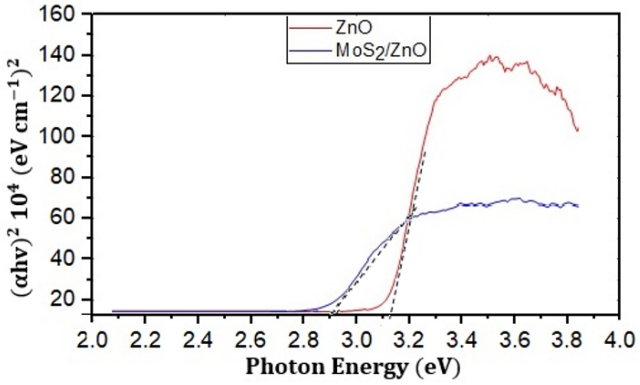

Fig. 6. Plots of the direct bandgap of pure ZnO and MoS_2/ZnO thin films

Refractive index (n) is an essential parameter for the building-up of the optical device. Moss $n = (\frac{95}{E_g})^{\frac{1}{4}}$ [24], and here $n = \sqrt{1 + (\frac{13.6}{E_g+3.47})^2}$ [25] proposed different models for relating the refractive index (n) to the optical band gap (E_g). The n values were obtained and given in Table 1. It can be seen that the Moss model gives the greater value of n by considering the sample bandgap.

Table 1. Bandgap and refractive index of pure ZnO and MoS_2/ZnO thin films

Samples	Crystallite size (nm)	Optical band gap (eV)	Refractive index (Mass)	Refractive index (Herve)
MoS_2/ZnO	42.67	2.90	2.39	2.35
ZnO	31.71	3.12	2.35	2.29

4.4. Photoluminescence (PL) Analysis

The ultraviolet (UV) luminescence emission corresponds to the near band edge (NBE) emission of ZnO is believed to be a result of the radiative recombination of free excitons in ZnO, whereas the visible emission is due to recombination of deep level (DL) defects and surface states [26].

Room temperature PL spectra of pure ZnO and MoS_2/ZnO are shown in Fig. 7. In this study, the samples displayed two distinct emissions under 325 nm excitation: a strong intensity emission that corresponds to the near band-edge emission and a broad peak due to intrinsic defects in the range from 420 nm to 630.

ZnO microrods emit a sharp and strong near-band edge (NBE) UV emission centered at around 385 nm with a FWHM of about 18 nm, along with a relatively weak broad visible emission band. The pure ZnO showed a strong UV emission peak centered at around 438 nm accounts for the near band edge which is mainly due to the recombination of electron-hole in ZnO [27], while the emission located at 537 nm is mostly ascribed to oxygen vacancies and zinc interstitials [28]. A Visible violet luminescence centered at 376 nm and a weak broad visible emission band, with the ultraviolet to visible luminescence ratio over 30, are recorded from MoS_2/ZnO. Compared with pure ZnO thin films, the UV emission of MoS_2/ZnO is increased by more than 1.5 times, while the DL emission is reduced.

One possible explanation for reduction of the visible luminescence intensity of MoS_2/ZnO is that the presence of oxygen vacancy defects decreases during MoS_2 decoration [29]. A remarkable blue-shift of the UV luminescence of MoS_2/ZnO seems to be the chance of the quenching of non-radiative recombination processes [30].

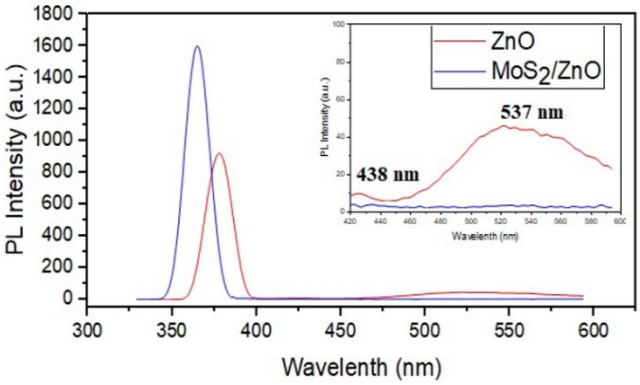

Fig. 7. PL emission spectra of pure ZnO and MoS_2/ZnO thin films under 325 nm excitation

To study separation mechanisms of photo-generated electrons and holes for MoS_2/ZnO composite, a possible diagram of the electron transfer mechanism is schematically drawn in Fig. 8.

We found that the optical bandgap of the ZnO/MoS_2 composite (2.90 eV) was lower than that of the pure ZnO (3.12 eV). Therefore, once a photon with energy greater than the band gap ($\lambda < 400$nm) is absorbed by the MoS_2/ZnO film, the electrons in the valence band (VB) of ZnO and MoS_2 can be promoted to the conduction band (CB).

When the MoS_2/ZnO film is illuminated with photons (2.90 eV < $h\nu$< 3.12 eV), the excited electrons on the VB of MoS_2 move to its CB and the electrons in the conductions band of ZnO can be trapped by defect centers (defect-related energy (DE) level). For wavelengths greater than 317 nm (photon energy<2.90 eV), the excited electrons still are able to transfer to the CB of MoS_2, and the energy level of the defect plays an essential role in electron-hole pair separation mechanism [30]. In this process, separation of the excited electrons and holes in the conduction band leads to a decrease in recombination rates and thus

improving the separation of the photo-generated electron-hole pairs and photocatalytic performance.

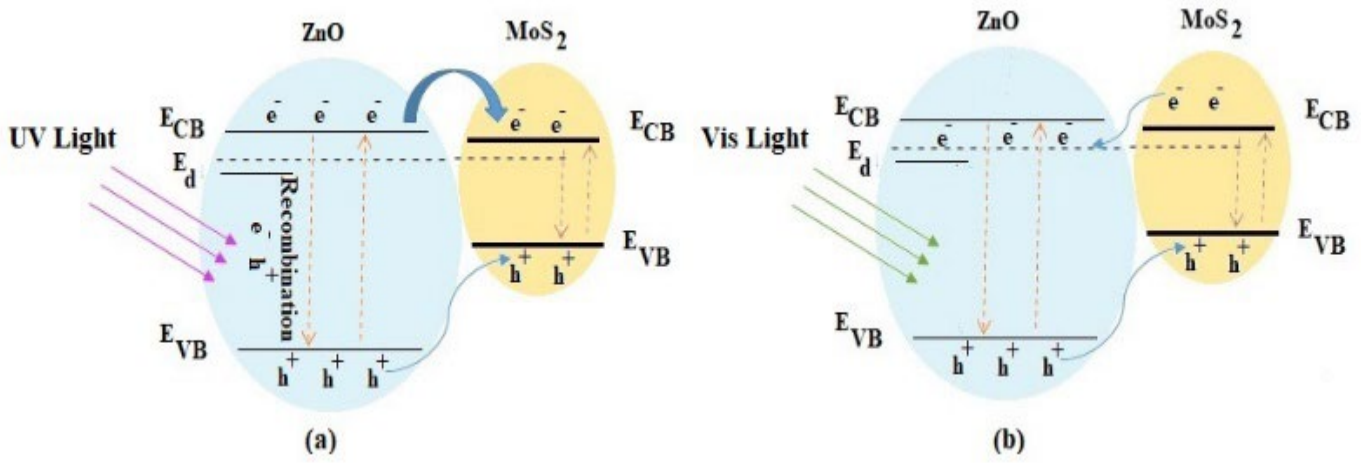

Fig. 8. Schematic illustration of the charge transfer process and energy level diagrams of pure ZnO and MoS_2/ZnO thin film

4.5. Electrical Properties

For the optoelectronic device applications, the current–voltage characteristics of MoS_2/ZnO film was investigated under UV illumination at 365 nm wavelength and in dark. The dependence of photo-current and dark-current on applied voltage is shown in Fig. 9 on a log–log scale. Each curve shows two straight lines having different slopes (r) for lower and higher voltage regions. According to the power-law relationship, $I \propto V^r$, if the slope of individual straight line is less than 1 (r<1), the dark-current and photo-current vary sub-linearly at lower voltage and above this voltage, the currents vary super-linearly (r>1). The transition of sub-linear to super-linear variation can be attributed to the trapped space charge–limited current inside the material [31].

In addition, electrical resistivity is an intrinsic property of a material that measures how strongly a material opposes the flow of electrical current. An analysis of electrical properties was conducted using an Ossila four-point probe. The average electrical resistivity of a thin film can be expressed as:

$$\rho = \frac{V\pi}{I \ln(2)} \qquad (3)$$

where ρ , V, and I are resistivity, applied voltage, and current, respectively. The average resistivity of pure ZnO thin film is $4.78 \times 10^4 \Omega m$. The resistivity of film decreases and reached $1.65 \times 10^3 \Omega m$ when MoS_2 has been deposited on ZnO microrods. As shown in Table 1, the crystallite size of MoS_2/ZnO is larger than that of pure ZnO film. Increasing the crystallite size leads to a decrease in the grain boundaries of MoS_2/ZnO film, resulting in higher mobility of electrons and conductivity of MoS_2/ZnO film [32], which provide a reference for micro–nano optoelectronic devices.

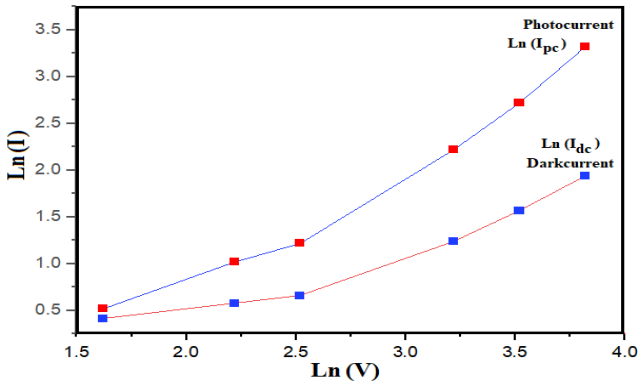

Fig. 9. Variation of photoelectric current (I) versus applied voltage for MoS_2/ZnO thin film

5. Growth Mechanism of ZnO Microrods

Pulsed laser deposition is a physical vapor deposition technique that utilizes a high-power pulsed laser beam in a vacuum chamber to eject material from a target in the form of a plasma plume in order to deposit on a substrate. The plume contains atomic and ionic components recondenses on a substrate. It is suitable for growth of multicomponent oxide thin films with controllable crystallinity and micro-nanoscale morphology.

As shown in Fig. 10, between two primary modes (Volmer-Weber and Stranski-Krastanov) by which thin films grow on a crystal surface or interface, the thin film growth by the Volmer-Weber growth mode is facilitated by the large lattice mismatch between ZnO film and the Si substrate. Small clusters or three-dimensional islands are first nucleated on the substrate because the cohesion between the adsorbed atoms is larger than the adhesion between the target atoms and the substrate.

As a result, the ZnO nanoparticles grow more rapidly along facets and have a stronger tendency to grow along the c-axis. The strong peak (002) implies highly oriented ZnO nanoparticles along the c-axis and the structure of ZnO is hexagonal wurtzite microrods. Sometimes, these microrods originate from a single center arranging them in a plane forming flower-like morphologies consisting of several microrods as shown in FESEM images.

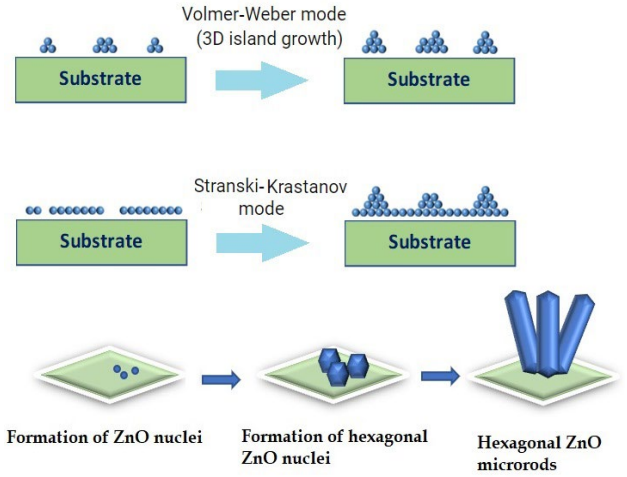

Fig. 10. Schematic illustration of two kinds of thin film growth modes and the possible growth mechanism for the formation of hexagonal microrods

6. Conclusion

In this work, MoS_2/ZnO microrods were successfully deposited on Si substrate by pulsed laser deposition method and a possible growth mechanism of microrods was illustrated. The average crystallite size of ZnO microrods increases with depositing MoS_2 layer on the prepared ZnO microrods, thus reducing the bandgap. The FESEM interpretation indicates that the surface of MoS_2/ZnO microrods shows more roughness and distortion in comparison with pure ZnO.

In UV–Vis experiments, decorating of MoS_2 on ZnO microrods reduced the optical band gap ranges from 3.12eV to 2.92 eV. The UV–Vis analysis reveals a red shift in the band gap of MoS_2/ZnO microrods. Compared with pure ZnO thin films, the UV emission of MoS_2/ZnO is increased by more than 1.5 times, while the DL emission is reduced. Such a heterostructure possesses a promising potential application prospect in various high-performance in optoelectronic devices.

Because adsorption, electron injection, and recombination occur at the surface of thin films, as a further progress of the research in the field of optoelectronic application, one of the key issues is the achievement of more improvement in terms of highly efficient light-emitting of surfaces and interfaces.

Declaration of Competing Interest

The authors have declared that no competing interests exist.

References

[1] Li, L., Xu, Y., Peng, Y., Fan, J., Zhang, H., Jin, L., Zou, Y. and Ma, X., 2024. Structural and optical properties of position-controlled n-ZnO nanowire arrays: Potential applications in optoelectronics. *Journal of Luminescence*, *268*, p.120399.

[2] Kamalianfar, A., Naseri, M., Abdala, A.A. and Jahromi, S.P., 2021. Hierarchical sphere-like ZnO–CuO grown in a controlled boundary layer for high-performance H_2S sensing. *Journal of Electronic Materials*, *50*(9), pp.5168-5176.

[3] Huang, W.L., Chu, S.Y. and Kao, P.C., 2022. Investigation of improving organic light-emitting diodes efficiency using an ultra-thin ultraviolet-ozone-treated Nb-doped ZnO film as anode buffer layer. *Journal of Alloys and Compounds*, *921*, p.166033.

[4] Kamalianfar, A., Naseri, M.G. and Jahromi, S.P., 2019. Preparation and gas-sensing performances of Cr_2O_3-decorated ZnO nanostructures grown in a boundary layer of non-uniform thickness for low-working temperature H_2S detection. *Chemical Physics Letters*, *732*, p.136648.

[5] Gudla, U.R., Suryanarayana, B., Raghavendra, V., Emmanuel, K.A., Murali, N., Taddesse, P., Parajuli, D., Naidu, K.C.B., Ramakrishna, Y. and Chandramouli, K., 2020. Optical and luminescence properties of pure, iron-doped, and glucose capped ZnO nanoparticles. *Results in Physics*, *19*, p.103508.

[6] Elkamel, I.B., Hamdaoui, N., Mezni, A., Ajjel, R. and Beji, L., 2023. Effects of plasmon resonance on the low frequency noise and optoelectronic properties of Au/Cu codoped ZnO based photodetectors. *Optical and Quantum Electronics*, *55*(2), p.148.

[7] Anandan, M., Dinesh, S., Christopher, B., Krishnakumar, N., Krishnamurthy, B. and Ayyar, M., 2024. Multifaceted investigations of co-precipitated Ni-doped ZnO nanoparticles: Systematic study on structural integrity, optical interplay and photocatalytic performances. *Physica B: Condensed Matter*, *674*, p.415597.

[8] Kamalianfar, A. and Naseri, M.G., 2019. Effect of boundary layer thickness on ammonia gas sensing of Cr_2O_3-decorated ZnO multipods. *Applied Physics A*, *125*(5), p.370.

[9] Ansari, N., Mohebbi, E. and Nazari, E., 2023. The role of the defect in photonic crystals based on WS_2 or WSe_2 monolayers: a vision on how to achieve high quality factor and wavelength adjustability in defect modes. *Optical and Quantum Electronics*, *55*(4), p.319.

[10] Alzaid, M., Hadia, N.M.A., Shaaban, E.R., El-Hagary, M. and Mohamed, W.S., 2022. Thickness controlling bandgap energy, refractive index and electrical conduction mechanism of 2D Tungsten Diselenide (WSe_2) thin films for photovoltaic applications. *Applied Physics A*, *128*, pp.1-12.

[11] Arora, A., Sharma, K. and Tripathi, S.K., 2023. Influence of precursors on hydrothermal synthesis and electronic properties of molybdenum diselenide. Applied Physics A, 129(9), p.654.

[12] Tyagi, P. and Choudhary, S., 2023. Uniaxial strain engineered MoS_2 (molybdenite) and chlorine adsorbed MoS_2 nanostructures for tuning their electronic and optical properties. *Optical and Quantum Electronics*, *55*(8), p.748.

[13] Liu, L., Ikram, M., Ma, L., Zhang, X., Lv, H., Ullah, M., Khan, M., Yu, H. and Shi, K., 2020. Edge-exposed MoS2 nanospheres assembled with SnS_2 nanosheet to boost NO_2 gas sensing at room temperature. *Journal of Hazardous Materials*, *393*, p.122325.

[14] Krishnan, U., Kaur, M., Kaur, G., Singh, K., Dogra, A.R., Kumar, M. and Kumar, A., 2019. MoS_2/ZnO nanocomposites for efficient photocatalytic degradation of industrial pollutants. *Materials Research Bulletin*, *111*, pp.212-221.

[15] Tang, C.M., Zhang, H.Y. and Zhang, J., 2020. Study on photocatalytic activity of MoS_2/ZnO composite in visible light. *Optoelectronics Letters*, *16*, pp.446-450.

[16] Liu, H.Q., Yao, C.B., Jiang, C.H. and Wang, X., 2021. Preparation, modification and nonlinear optical properties of semiconducting MoS_2 and MoS_2/ZnO composite film. *Optics & Laser Technology*, *138*, p.106905.

[17] Aliannezhadi, M., Mirsanai, S.Z., Jamali, M. and Tehrani, F.S., 2024. Optical and structural properties of bare MoO_3 nanobelt, ZnO nanoflakes, and MoO_3/ZnO nanocomposites: The effect of hydrothermal reaction times and molar ratios. *Optical Materials*, *147*, p.114619.

[18] Doiphode, V., Shinde, P., Punde, A., Shah, S., Kale, D., Hase, Y., Ladhane, S., Rahane, S., Waghmare, A., Bade, B. and Rondiya, S., 2024. Solution-processed synthesis of ZnO/CdS heterostructure photoanode for efficient photoelectrochemical water splitting. *Journal of Power Sources*, *609*, p.234712.

[19] Zhao, Y., Xu, B., Tong, L. and Zhang, J., 2022. The helicity of Raman scattered light: principles and applications in two-dimensional materials. *Science China Chemistry*, *65*(2), pp.269-283.

[20] Liu, H.Q., Yao, C.B., Jiang, C.H. and Wang, X., 2021. Preparation, modification and nonlinear optical properties of semiconducting MoS_2 and MoS_2/ZnO composite film. *Optics & Laser Technology*, *138*, p.106905.

[21] Tkachenko, D., Kochnev, N., Bobrysheva, N., Osmolowsky, M., Voznesenskiy, M. and Osmolovskaya, O., 2023. Influence of doping with Co, Cu and Ni on the morphological and structural parameters and functional properties of ZnO nanoobjects. *Materials Chemistry and Physics*, *308*, p.128307.

[22] Benavente, E., Durán, F., Sotomayor-Torres, C. and González, G., 2018. Heterostructured layered hybrid ZnO/MoS_2 nanosheets with enhanced visible light photocatalytic activity. *Journal of Physics and Chemistry of Solids*, *113*, pp.119-124.

[23] Wang, S., Ren, C., Tian, H., Yu, J. and Sun, M., 2018. MoS_2/ZnO van der Waals heterostructure as a high-efficiency water splitting photocatalyst: A first-principles study. *Physical Chemistry Chemical Physics*, *20*(19), pp.13394-13399.

[24] Al-Shemri, M.I., Aliannezhadi, M., Ghaleb, R.A. and Al-Awady, M.J., 2024. Au-$H_2Ti_3O_7$ nanotubes for non-invasive anticancer treatment by simultaneous photothermal and photodynamic therapy. *Scientific Reports*, *14*(1), p.25998.

[25] Zakaly, H.M., Issa, S.A., Saudi, H.A., Algethami, M. and Soliman, T.S., 2024. Enhancing optical and radiation shielding properties: A dive into Bi_2O_3-Infused glasses. *Optical Materials*, *152*, p.115496.

[26] Bouderbala, I.Y., Guessoum, A., Rabhi, S., Bouhlassa, O. and Bouras, I.E., 2024. Optical band-diagram, Urbach energy tails associated with photoluminescence emission in defected ZnO thin films deposited by sol–gel process dip-coating: effect of precursor concentration. *Applied Physics A*, *130*(3), p.205.

[27] Kumar, D., Singh, M.K. and Mehata, M.S., 2022. Exploration of grown cobalt-doped zinc oxide nanoparticles and photodegradation of industrial dye. *Materials Research Bulletin*, *150*, p.111795.

[28] Lei, M.Y., Liu, C.M., Zhou, Y.G., Yan, Z.H., Han, S.B., Liu, W., Xiang, X. and Zu, X.T., 2016. Microstructure and photoluminescence of MoS_2 decorated ZnO nanorods. *Chinese journal of physics*, *54*(1), pp.51-59.

[29] Yao, C., Lin, J., Qu, Y., Jiang, K., Hu, Z., Li, L., Xu, N., Sun, J. and Wu, J., 2022. WS_2-decorated ZnO nanorods and enhanced ultraviolet emission. *Materials Letters*, *306*, p.130880.

[30] Rahimi, K., Moradi, M., Dehghan, R. and Yazdani, A., 2019. Enhancement of sunlight-induced photocatalytic activity of ZnO nanorods by few-layer MoS2 nanosheets. *Materials Letters*, *234*, pp.134-137.

[31] Prabhu, N.S., Sharmila, K., Karunakara, N., Sayyed, M.I., Almuqrin, A.H. and Kamath, S.D., 2022. Consequences of doping Er^{3+} and Yb^{3+} ions on the thermoluminescence dosimetry performance of the BaO-ZnO-LiF-B_2O_3-Sm_2O_3 glass system. *Journal of Non-Crystalline Solids*, *582*, p.121460.

[32] Khan, M.I., Ali, S., Alwadai, N., Irfan, M., Albalawi, H., Almuqrin, A.H., Almoneef, M.M. and Iqbal, M., 2022. Structural, electrical and optical properties of hetrostructured MoS_2/ZnO thin films for potential perovskite solar cells application. *Journal of Materials Research and Technology*, *20*, pp.1616-1623.